

Surface geometry of BaO on W(100): A surface-extended x-ray-absorption fine-structure study

A. Shih, C. Hor, W. Elam, and J. Kirkland
Naval Research Laboratory, Washington, DC 20375-5000

D. Mueller

National Institute of Standards and Technology, Gaithersburg, Maryland 20899

(Received 30 October 1990; revised manuscript received 29 April 1991)

A surface-extended x-ray-absorption fine-structure study of ordered monolayers of coadsorbed barium and oxygen on a single-crystal W(100) surface is described. A $(\sqrt{2} \times \sqrt{2})R45^\circ$ structure with a stoichiometric barium-to-oxygen ratio, and a $(2\sqrt{2} \times \sqrt{2})R45^\circ$ structure with a nearly 1:2 barium-to-oxygen atomic ratio both form on W(100). The surface-extended x-ray-absorption fine-structure results indicate that all the barium and oxygen atoms are nearly coplanar in the $(\sqrt{2} \times \sqrt{2})R45^\circ$ overlayer. The Ba-to-O distance in this overlayer is $3.20 \pm 0.05 \text{ \AA}$ and $\beta = 82^\circ \pm 5^\circ$, where β is the angle between the Ba-O internuclear axis and the surface normal. For the $(2\sqrt{2} \times \sqrt{2})R45^\circ$ overlayer, there are two types of oxygen sites. Oxygen atoms nearly coplanar with the barium atoms are also present in these films with a Ba-to-O distance of $3.27 \pm 0.05 \text{ \AA}$ and $\beta = 75^\circ \pm 4^\circ$. Additional oxygen atoms lie outside the barium plane at a distance $2.03 \pm 0.05 \text{ \AA}$ and $\beta = 23^\circ \pm 10^\circ$ from the nearest barium atoms.

I. INTRODUCTION

The geometry of BaO adsorbed on tungsten substrates is an interesting and challenging problem amenable to surface-extended x-ray-absorption fine-structure (SEXAFS) analysis. Barium oxide adsorption behavior represents a technologically important problem; a monolayer of barium oxide adsorbed on tungsten is the essential work-function-lowering feature present on dispenser cathode surfaces. Such cathodes are widely used in high-power microwave tubes. Dispenser cathodes make use of adsorbed barium oxide monolayers both because they are characterized by a low work function, and because barium oxide monolayers are quite stable thermally. (Cs-O covered surfaces, for example, may exhibit lower work-function values; however, upon heating Cs desorbs too readily for these surfaces to be useful as thermionic emitters.) A knowledge of the surface geometry of BaO adsorbed on W surfaces is important in understanding the origin of the strong binding as well as the work-function-lowering mechanism.

Because many closely spaced core levels are found below 2 keV in Ba and W atoms, the measurement must be performed at high energy—either above the Ba K or the Ba L_3 edge. The L_3 edge was employed in the work describe here. Most SEXAFS experiments have been performed at lower energies.¹

Surface barium oxide layers contain barium in a rather different environment than environments found in bulk barium compounds; thus the data analysis may encounter difficulties with the breakdown of extended x-ray-absorption fine-structure (EXAFS) phase and amplitude transferability.^{2,3} To take this possibility into account we obtained reference data for a variety of barium containing bulk compounds. BaO and BaWO₄ were employed as standards in the final analysis because self-consistent re-

sults were obtained when the analysis was performed using these reference compounds.

SEXAFS does not require specimens exhibiting long-range order, thus the technique may be applied to the study of polycrystalline surfaces such as those found on dispenser cathodes. Norman *et al.*⁴ performed a SEXAFS investigation of a dispenser cathode surface. Norman proposed a model of the adsorption geometry with the barium-oxygen interatomic axis normal to the surface. Shih *et al.*⁵ also examined barium oxide adsorption on polycrystalline tungsten by SEXAFS but obtained a radically different result. The reports found different bond-length values and coordination numbers and even differed in the identification of the next-nearest-neighbor species. Shih *et al.* proposed an entirely different adsorption geometry with a tilted barium-oxygen interatomic axis. Both groups recognized the inherent difficulty in reconstructing the adsorption geometry from SEXAFS measurements on polycrystalline substrates. The measured bond-length values and the coordination numbers were averaged over an unknown distribution of crystal faces.

To avoid this difficulty studies employing single-crystal substrates are required. The high symmetry of the W(100) face facilitates theoretical treatment. Quantum theoretical calculations for BaO adsorption on W(100) has been pursued independently by two different approaches, full-potential linear augmented-plane-wave (FLAPW) calculations^{6,7} and cluster calculations.⁸ Experimental studies⁹⁻¹¹ indicate that a well-ordered BaO layer characterized by a $c(2 \times 2) = (\sqrt{2} \times \sqrt{2})R45^\circ$ low-energy electron diffraction (LEED) pattern may be grown on W(100). The $c(2 \times 2)$ overlayer corresponds to a coverage level of $\sim 5 \times 10^{14}$ barium atoms/cm² and $\sim 5 \times 10^{14}$ oxygen atoms/cm². Only one barium and one oxygen atom occupy each overlayer unit cell. A

FLAPW total-energy calculation⁷ predicts that the barium and oxygen adatoms are nearly coplanar, with the Ba–O internuclear axis tilted by 16° off coplanar.

In studies of ordered overlayers it is useful to examine the polarization dependence of the SEXAFS signal. The polarization dependence provides a direct determination of the orientation of the Ba–O internuclear axis relative to the surface normal. This dependence is a direct consequence of the preferred direction of photoelectron emission for the linearly polarized synchrotron light (i.e., the EXAFS signals are strongly enhanced when the polarization vector is directed along the internuclear axis).

II. EXPERIMENTAL SETUP AND OVERLAYER PREPARATION

The SEXAFS measurements were performed in an ultrahigh vacuum chamber attached to beam line X23B of the National Synchrotron Light Source at Brookhaven National Laboratory. The monochromator type and focusing arrangement, as well as measurements of the energy resolution and degree of polarization of the beamline, have been reported previously.¹² A description of the end station has been given in a prior publication.⁵ The total electron yield (the total sample photocurrent) was recorded above and below the Ba L_3 edge (~ 5247 eV). The x-ray flux was monitored by an in-line ion chamber located immediately before a Be entrance window on the ultrahigh vacuum chamber. The W(100) single crystal was mounted so that its vertical rotation axis was within the plane of the sample surface. This geometry facilitated rotation of the surface normal with respect to the horizontal polarization vector of the linearly polarized incident synchrotron beam.

The overlayers were prepared *in situ*. The experimental chamber was equipped with both a BaO evaporator for deposition of BaO and a Ba evaporator for metallic barium evaporation. Prior to deposition of an overlayer the tungsten crystal was cleaned by annealing at 2300 K for 20 sec. To monitor surface cleanliness Auger-electron spectra were obtained before and after each SEXAFS measurement. At the background pressure (5×10^{-11} Torr during the SEXAFS measurements) about 10% of a Ba monolayer becomes oxidized during exposure to residual gases for 3 h. The oxide overlayers were less reactive. No significant changes in the Auger-electron Spectroscopy (AES) data were noted during the hour required for acquisition of a typical SEXAFS spectrum.

A combined LEED and AES study¹¹ determined that several well-ordered coadsorbed barium and oxygen overlayers form on the W(100) substrate. Those chosen for SEXAFS examination were as follows: a stoichiometric BaO overlayer characterized by a $(\sqrt{2} \times \sqrt{2})R45^\circ$ LEED pattern, and an overlayer with two oxygen atoms per barium atom which exhibits a $(2\sqrt{2} \times \sqrt{2})R45^\circ$ LEED pattern. The LEED and AES study¹¹ prescribed reproducible procedures to form either of the two ordered structures. As a clean W(100) surface, held at 860°C, is exposed to a barium oxide flux initial deposition is stoichiometric. At exposure levels beyond that required to complete the $(\sqrt{2} \times \sqrt{2})R45^\circ$ overlayer further barium

oxide exposure increases the oxygen coverage but not the barium coverage. The oxygen coverage saturates when about twice as many oxygen atoms are present as in the stoichiometric barium oxide overlayer. In this experiment, a 4-min evaporation period was required to deposit a stoichiometric BaO overlayer to full coverage. Evaporation periods of ~ 15 min were required, to produce the $(2\sqrt{2} \times \sqrt{2})R45^\circ$ structure. The ordered metallic Ba adlayer [also in the $(\sqrt{2} \times \sqrt{2})R45^\circ$ structure] was produced by annealing a barium film several layers thick at 800°C for 2 min. On the basis of LEED and AES experiments,¹¹ we know that following this treatment all but the first saturated monolayer of the multilayer film has desorbed.

III. SEXAFS RESULTS AND DATA ANALYSIS

X-ray-absorption spectra for the three ordered overlayers are shown in Fig. 1. The oscillations are strongest in the spectrum for the $(2\sqrt{2} \times \sqrt{2})R45^\circ$ overlayer and weakest for the barium metal overlayer where the oscillations are not clearly visible on the scale shown. The reproducibility of the Ba overlayer data was not sufficient to determine the adsorption geometry of the barium atoms; however, these data did reveal that backscattering from the substrate tungsten atoms was not important in contributing to the main features found in the Fourier transforms of the oxygen-containing overlayer EXAFS signals. In this experiment the relative absorption amplitude above the Ba L_3 adsorption edge (~ 5247 eV) was measured, thus the local geometry around the Ba atoms was investigated.

Quantitatively the oscillatory EXAFS function $\chi(k)$ is given by

$$\chi(k) = \sum_i N_i^* A_i \sin[2kR_i + \phi_i(k)]. \quad (1)$$

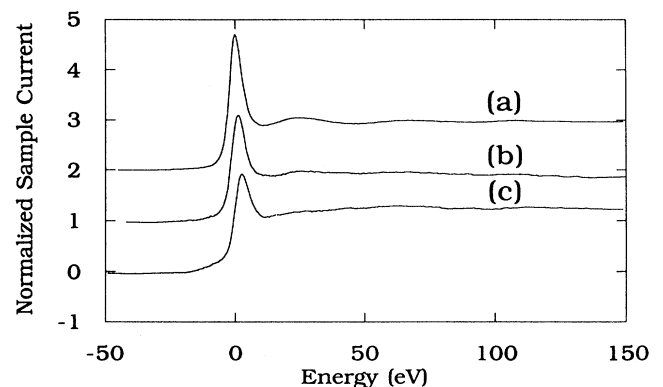


FIG. 1. Absorption spectra near the Ba L_3 edge, taken at normal incidence, for (a) a nonstoichiometric barium oxide overlayer with excess oxygen $W(100)-(2\sqrt{2} \times \sqrt{2})R45^\circ$ (b) a stoichiometric barium oxide monolayer $W(100)-(\sqrt{2} \times \sqrt{2})R45^\circ$ -BaO, (c) a barium monolayer $W(100)-(\sqrt{2} \times \sqrt{2})R45^\circ$ -Ba. The EXAFS oscillations are strongest for the overlayer with excess oxygen, and weakest for the overlayer devoid of oxygen. The spectra were normalized to unit step edge and offset vertically.

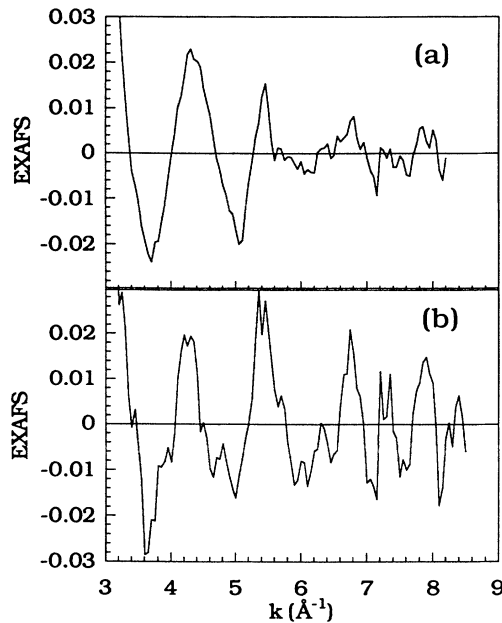


FIG. 2. The oscillatory part of EXAFS, $\chi(k)$, after normalization to unit edge step and removal of cubic spline background, and conversion to k space for the absorption spectra (a) and (b) of Fig. 1, respectively.

The summation extends over all neighbor shells separated from the absorbing atom by a distance R_i . ϕ_i is the total phase shift which the photoelectron experiences during the absorbing and backscattering process. For K and L_1 edges the product $N_i^* A_i$ is the total backscattering amplitude. For L_2 and L_3 edges, the equation must be modified as discussed below. Figure 2 shows the oscillatory part of EXAFS, $\chi(k)$, for the two mixed barium and oxygen layers taken at normal incidence. The curves show the data following normalization to unit step-edge height, removal of a cubic spline background, and conversion to k space.¹³ The curve in 2(a) is for the layer with excess oxygen $W(100)-(2\sqrt{2}\times\sqrt{2})R45^\circ$, and the curve in 2(b) is for the stoichiometric layer, $W(100)-(\sqrt{2}\times\sqrt{2})R45^\circ\text{-BaO}$. Each spectrum was the result of a single run. In the k -space conversion, E_0 was taken at the point corresponding to half the step-edge height.

A. Radial distributions

The various neighbor shells can be sorted out by Fourier transformation of the EXAFS signal $\chi(k)$ which yields the radial distribution function. Structural differences between the $(\sqrt{2}\times\sqrt{2})R45^\circ$ and $(2\sqrt{2}\times\sqrt{2})R45^\circ$ barium and oxygen overlayers are clearly evident in Fig. 3 which compares the k^2 -weighted Fourier-transformed EXAFS spectra of the two over-

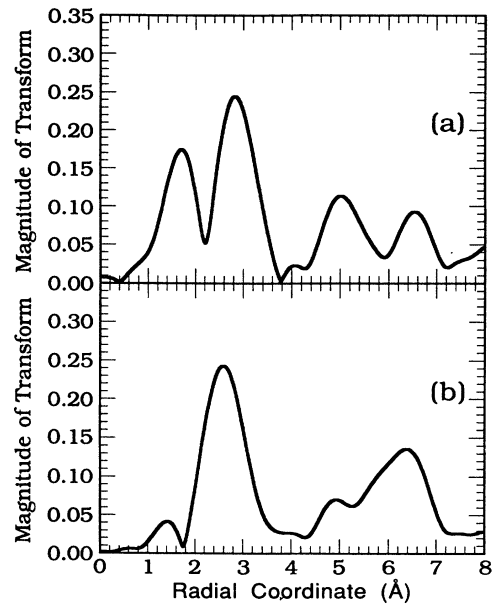


FIG. 3. k^2 -weighted Fourier transforms of SEXAFS spectra from (a) a stoichiometric BaO overlayer $W(100)-(\sqrt{2}\times\sqrt{2})R45^\circ\text{-BaO}$ and (b) an overlayer saturated with excess oxygen $W(100)-(2\sqrt{2}\times\sqrt{2})R45^\circ$. The peak near 2 Å is attributed to those oxygen neighbors which are present only in the overlayer with excess oxygen.

layers. It is immediately obvious from this comparison that the excess oxygen atoms in the $(2\sqrt{2}\times\sqrt{2})R45^\circ$ overlayer give rise to the feature below 2 Å. A feature near 3 Å, present in spectra from both overlayers, arises mainly from oxygen neighbors at a larger distance than the excess oxygen atoms. The backreflection from this shell of oxygen dominates the EXAFS of the stoichiometric layer. Further evidence supporting the identification of the atoms producing the 3-Å peak in the radial distribution function as oxygen will be discussed later.

The clear separation of the two oxygen shells facilitates the analysis greatly. Possible interference effects are considered at the end of the discussion section. These two oxygen shells differ not only in their distance from the barium but also exhibit entirely different polarization angle dependence.

B. Polarization dependence

N^* in Eq. (1) is the effective coordination number. For L_2 and L_3 edges it is given by^{14,15}

$$N^* = N_0[(0.5+c) + (1.5-3c)\cos^2\alpha] \quad (2)$$

Here N_0 is the actual number of neighbors, α is the angle between the electric field \mathbf{E} of the incident beam and the internuclear axis between the absorbing atom and the backreflecting neighbor, and c is a final-state parameter.

In general, linear polarization of the incident x-ray beam can have a strong effect on the resultant EXAFS signal as indicated by the cosine-squared term. A neighbor contributes significantly to the EXAFS signal only if the electric field has a sizable component along the position vector connecting the neighbor and the absorber. This effect is useful in the determination of bond directions.

EXAFS analysis above an L_2 or an L_3 edge is complicated by interference between two dipole-allowed final states ($l=0$ and $l=2$). Although the $l=2$ final-state dominates, the $l=0$ state introduces an additional term c into Eq. (2). c is the ratio of the transition-matrix elements for transitions into s and d final states, and is in general approximately 0.2.¹⁵ The s , d final-state interference can also lead to errors in the derived bond length. Fortunately, the absolute coordination number can be obtained *directly* (i.e., $N^*=N_0$) from a surface EXAFS measurement recorded at the x-ray incidence angle 54.7° (the angle θ between the \mathbf{E} vector and the surface normal) provided the surface geometry has threefold or higher symmetry.¹⁴ [Substitution of $\theta=54.7^\circ$ in Eqs. (3) and (2) yields $N^*=N_0$. Note that from LEED we know that for the $(2\sqrt{2}\times\sqrt{2})R45^\circ$ overlayer there are four equivalent domains with the Ba nearest oxygen orientation rotated azimuthally by 90° . For the $(\sqrt{2}\times\sqrt{2})R45^\circ$ overlayer the diffraction pattern requires either a fourfold symmetry of oxygens around a barium or that there are four equivalent domains rotated by 90° .] For each of the BaO overlayers, SEXAFS spectra were recorded near this angle. (In practice, the spectra were taken at 57° , instead of the exact "magic angle" to avoid a Bragg reflection from the substrate. This small difference in angle is expected to have no significant effect.) For the polarization-dependence study additional EXAFS spectra were collected at $\theta=90^\circ$ (normal incidence of the x-ray beam) and at $\theta=30^\circ$. (To obtain a stronger polarization effect, a shallower grazing angle is preferred; however, substrate Bragg reflections limited us to $\theta\geq 30^\circ$.)

Fourier transforms of the EXAFS spectra for the $(2\sqrt{2}\times\sqrt{2})R45^\circ$ overlayer, taken at $\theta=90^\circ$, 57° , and 30° , are shown in Fig. 4 to illustrate the effect of the polarization on the two oxygen shells. Clearly the "excess oxygen" peak near 2 Å increases in height as the angle of incidence changes from normal incidence to a more grazing angle. This reveals that the position vector from the barium to the excess oxygen is more nearly upright than in the surface plane. In contrast, the next-nearest oxygen atom shell, which is present for the stoichiometric overlayers as well, decreases in height in the same sequence. This indicates a more co-planar geometry.

The angular dependence of the effective coordination number N^* in Eq. (2) is expressed in terms of the angle α between the polarization vector and the bond direction. To facilitate interpretation of the experimental results the angular dependence can be expressed in terms of the angle β between the surface normal and the barium-oxygen internuclear axis, and the angle θ between the polarization vector and the surface normal [see Fig. 5(a)]. Performing an average over the azimuthal orientation of four equivalent domain types (indicated by LEED) for the polarization vector and the internuclear orienta-

tion yields

$$\cos^2\alpha = \cos^2\theta \cos^2\beta + \frac{1}{2} \sin^2\theta \sin^2\beta. \quad (3)$$

Figure 5(b) illustrates the calculated N^*/N_0 ratio as a function of θ for several values of β . Also indicated are the observed changes in the Fourier-transform peak heights for the two oxygen peaks in the EXAFS data from the $(2\sqrt{2}\times\sqrt{2})R45^\circ$ overlayer. Note that $\beta=0^\circ$ corresponds to a barium-oxygen internuclear axis normal to the surface while $\beta=90^\circ$ corresponds to a barium-oxygen axis parallel to the plane of the surface. A least-squares fit of the observed polarization dependence yields a bond angle of $23\pm 10^\circ$ for the closest oxygen neighbor, and $71\pm 10^\circ$ for the second-nearest oxygen neighbor. Here we have assumed a value of 0.2 for c . The ratio c has been calculated for a variety of elements and was found to be approximately 0.2 for $Z\geq 20$.¹⁵ Note that the bond angles determined in this manner are not very sensitive to the precise knowledge of the c value. Even

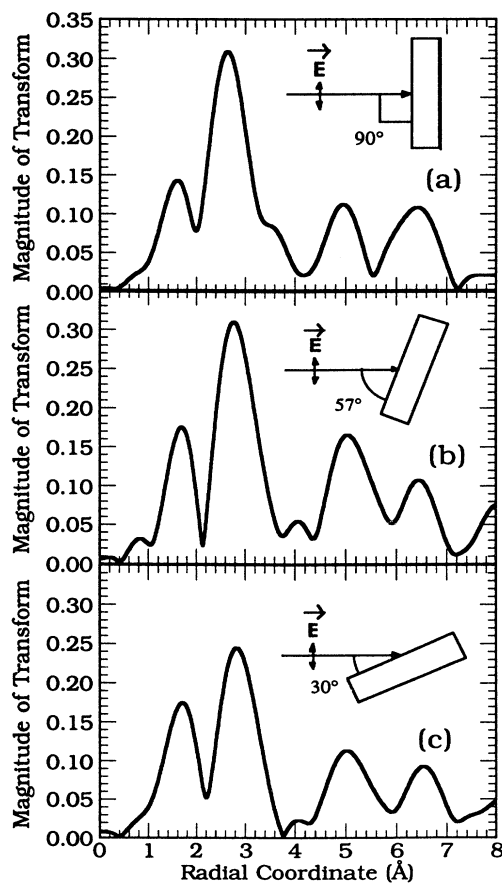


FIG 4. k^2 -weighted Fourier transforms of SEXAFS data from a $(2\sqrt{2}\times\sqrt{2})R45^\circ$ overlayer collected at various incidence angles. The polarization dependence of the first two features is clearly different. The polarization angles θ are 90° , 57° , and 30° in (a), (b), and (c), respectively.

with $c = 0$, i.e., purely d final state, the derived bond angles are $\beta = 37^\circ$ for the nearest oxygen, and $\beta = 64^\circ$ for the second oxygen shell.

For the oxygen in the second nearest shell the bond angle can also be determined from the measured Ba to O bond length of $3.27 \pm 0.05 \text{ \AA}$ (see below). In order to be in registry with the long-range order of the $(2\sqrt{2} \times \sqrt{2})R45^\circ$ overlayer a tilted geometry with $\beta = 75 \pm 4^\circ$ is required. The close agreement between this value and the 71° value obtained on the basis of the polarization dependence indicates that 0.2 was a good estimate for c .

The polarization dependence observed for the $(\sqrt{2} \times \sqrt{2})R45^\circ$ overlayer was similar to that observed for the second oxygen shell in the $(2\sqrt{2} \times \sqrt{2})R45^\circ$ overlayer. The measurements were not repeated with sufficient statistics to permit a reliable determination of the barium-oxygen orientation by the angular dependence as illustrated in Fig. 5 for the $(2\sqrt{2} \times \sqrt{2})R45^\circ$

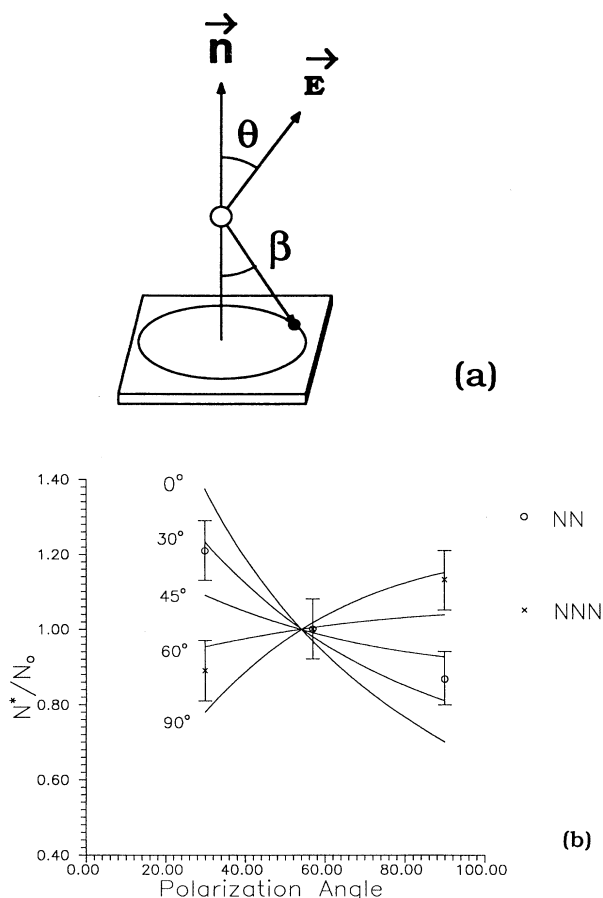


FIG. 5. The definitions of the polarization angle θ and the bond angle β are shown in (a). The polarization dependence for the first two Fourier-transform peaks for the $(2\sqrt{2} \times \sqrt{2})R45^\circ$ overlayer data are plotted as a function of the polarization angle together with the calculated polarization dependence for several adsorption geometries (b).

overlayer; however, the angle β is constrained to $82 \pm 5^\circ$ by the measured barium-oxygen distance, coordination number information, and the long-range order of the $(\sqrt{2} \times \sqrt{2})R45^\circ$ overlayer.

C. Bond lengths and coordination numbers

To determine the interatomic spacings and coordination numbers, we have adopted a theory-independent approach that relies on comparison with a model compound of known crystal structure for implicit information about the phase shifts $\phi(k)$ and backscattering amplitudes $A(k)$.^{2,3} This approach avoids the need for a direct measurement of the kinetic energy origin E_0 which is required in the conversion of the kinetic energy to wave vector k . If k is expressed in \AA^{-1} and energy in eV

$$k = 0.5123(E - E_0)^{1/2}. \quad (4)$$

The shift in core-level binding energy between the unknown and the model compound can be determined in the following self-consistent fashion (see, for example, Ref. 16). The unknown bond length R_x can be calculated from

$$R_x = (2kR_s + \delta_x - \delta_s) / 2k', \quad (5)$$

where δ_x and δ_s are the phase shifts for the unknown and the standard, respectively, as determined experimentally by Fourier filtering and back transformation; R_s is the known bond length in the standard, and

$$k' = 0.5123(E - E_0 - \Delta)^{1/2}. \quad (6)$$

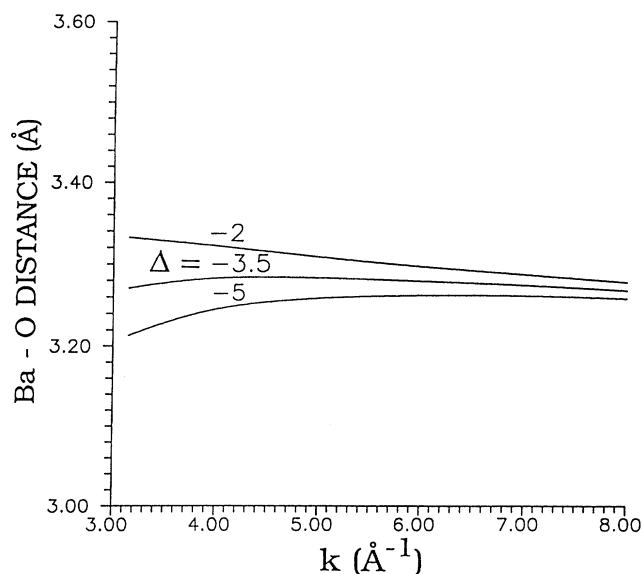


FIG. 6. The bond length R_x from barium to the next-nearest oxygen neighbor for a $(2\sqrt{2} \times \sqrt{2})R45^\circ$ overlayer calculated as a function of the wave vector based on Eq. (5). BaWO_4 was used as the model compound. The calculation is shown for several values of Δ . The proper choice of Δ makes R_x independent of the wave vector k .

TABLE I. The bond-length values and coordination numbers for the two ordered coadsorbed barium and oxygen overlayers on W(100).

	Stoichiometric BaO ($\sqrt{2} \times \sqrt{2}$)R45°		BaO with excess oxygen ($2\sqrt{2} \times \sqrt{2}$)R45°	
	R	N	R	N
Nearest neighbor	3.20±0.05 Å	3.0±0.8	2.03±0.05 Å	0.8±0.4
Next-nearest neighbor			3.27±0.05 Å	3.6±0.6

The inner potential difference Δ is a consequence of the core-level binding-energy shift between the reference material and the sample. For a proper choice of Δ R_x should be a constant independent of k . In Fig. 6 the derived distance between the barium and the next-nearest oxygen neighbors in a ($2\sqrt{2} \times \sqrt{2}$)R45° overlayer is plotted as a function of k . The standard used for this illustration was BaWO₄. In this self-consistent fashion, R_x and Δ were determined as 3.27 Å and -3.5 eV respectively.

An approach that sets the intercept of the phase difference between the unknown and the standard to zero³ was also used. No significant difference in the bond length was found. The amplitude ratio technique^{2,17} was used for coordination number determination. The bond length and coordination number results are summarized in Table I. Data from $k = 3.2$ to 8.2 \AA^{-1} weighted by k^2 were included in the Fourier transform. R -space windows were 1.0 to 2.2 Å for the nearest neighbor, and 2.2 to 3.4 Å for the next-nearest neighbors. Two model compounds, BaO and BaWO₄, were used in the data analysis. There are six oxygen atoms at 2.76 Å in the first shell neighbor for barium in bulk BaO.¹⁸ There are four oxygen atoms at 2.61 Å and four oxygen atoms at 2.77 Å for barium in BaWO₄.¹⁸ These two shells are too close to be resolved, and weighted averages of $\bar{R} = 2.69 \text{ \AA}$ and $\bar{N} = 7.8$ were used for the radial distance and coordination number in the analysis. The minimum in the amplitude (beat mode) caused by the interference of the two closely spaced shells occurs at $\sim 10 \text{ \AA}^{-1}$, which is outside our data range. The effect of this symmetric disorder introduces $\sigma^2 = 0.0064 \text{ \AA}^{-2}$ to the overall Debye-Waller factor, which we estimate to be 0.012 \AA^{-2} , comparable to what was observed in the oxygen shell of the bulk BaO or in the oxygen shells under study.

IV. DISCUSSION

In the analysis approach adopted here, phase and amplitude transferability from the model compound to the unknown is assumed. For accurate interatomic distance and coordination number determination the local environment of the atom pairs should be similar in the standard and the unknown. This is not necessarily the case for the bulk BaO standard and the surface BaO overlayers. Bulk BaO is an ionic compound in which the Ba atoms transfer most of their 6s electrons to the oxygen

atoms. An analysis of the low-energy Auger spectrum of a BaO monolayer adsorbed on W(100) indicated that the Ba atoms in the overlayers retained most of their 6s bonding electrons.¹⁹ This ionicity difference may be the reason for the large inner potential differences [~ 12 eV for the ($2\sqrt{2} \times \sqrt{2}$)R45° overlayer and ~ 18 eV for the ($\sqrt{2} \times \sqrt{2}$)R45° overlayer] obtained when overlayer spectra were analyzed with bulk BaO as the standard. The principle of phase and amplitude transferability has not been tested for systems with such large inner-potential differences.³ Using BaWO₄ as the model compound produced much smaller inner-potential differences [~ 4 eV for the ($2\sqrt{2} \times \sqrt{2}$)R45° overlayer and ~ 10 eV for the ($\sqrt{2} \times \sqrt{2}$)R45° structure]. Interatomic spacings derived using the two standards agreed to within 0.03 Å, with the slightly larger values obtained using BaWO₄ as the standard. Differences in the experimentally derived coordination numbers were not significant. Use of data from the bulk BaO standard was preferred for the analysis of the “excess oxygen” features for the ($2\sqrt{2} \times \sqrt{2}$)R45° overlayer data. Here the inner-potential difference was less than 2 eV.

A FLAPW calculation,⁶ which assumed a fourfold-hollow adsorption site, predicted a tungsten-atom-barium-atom separation of 3.3 Å, which is very close to the “in-plane” oxygen distance measured here. Several features of the analysis indicate that the 3-Å feature in the Fourier transform originates mainly from oxygen backreflection and not from tungsten. For example, the envelope function in Fourier filtering of the feature exhibits an oxygen-like backreflection. It is very different in functional form from the tungsten backreflection envelope.²⁰ The nearly constant $R_x(k)$ values in Fig. 6 indicate that the phase shift in the atomic pair, which gives rise to the 3-Å feature, is very similar to the Ba-O phase shift in the model compound. Furthermore, the polarization-dependence study indicates that atoms in the shell associated with the 3-Å feature are nearly coplanar with the barium atom—the tungsten substrate atoms are beneath the barium atoms.

It is known that Ramsauer-Townsend resonance, which typically occurs in the backscattering phase shift and amplitude of high- Z atoms, often introduces a large satellite peak at small distance in Fourier-transformed EXAFS spectra.²¹ The absence of a significant satellite peak (see Fig. 3) provides additional evidence that the

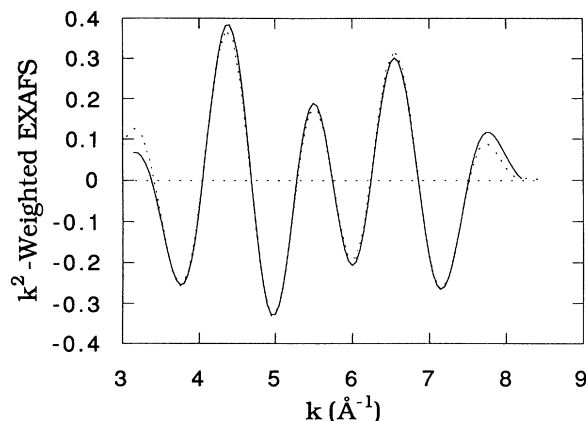


FIG. 7. Bond-length and coordination number determination through curve fitting. The solid curve is the Fourier-filtered EXAFS including both oxygen neighbor peaks for the $W(100)-(2\sqrt{2}\times\sqrt{2})R45^\circ$ overlayer. The dashed curve was calculated for barium atoms surrounded by two oxygen shells: $R_1=2.03$ Å, $N_1=0.6$ and $R_2=3.26$ Å, $N_2=4.2$. Experimental reference data for $BaWO_4$ was used in the calculation.

tungsten contribution to the EXAFS signal is not appreciable. Finally, calculations using the McKale table²⁰ indicate that in the range of 3 to 8 Å⁻¹ the total signal is dominated by the oxygen shell to within the error bar. Over this range, the signal from the tungsten shell is much smaller than the oxygen shell.

Because of the proximity of the first two features in the Fourier transform of the $(2\sqrt{2}\times\sqrt{2})R45^\circ$ monolayer data (Fig. 3), interference between the two peaks could shift the peak positions significantly. We have used a curve-fitting program²² to analyze the Fourier-filtered spectra with a window enclosing both peaks. The results of the data analysis performed in this way agree well with the values listed in Table I. Figure 7 shows an example of the curve fitting; the solid curve is the Fourier-filtered experimental data for the $(2\sqrt{2}\times\sqrt{2})R45^\circ$ overlayer while the dashed curve is least-square fit composite for two oxygen-neighbor shells. The least-squares fit, which uses phases from $BaWO_4$, yields $R_1=2.03$ Å, $N_1=0.6$ for the first oxygen-neighbor shell and $R_2=3.26$ Å, $N_2=4.2$ for the second oxygen shell. Analysis of the isolated peaks for the same spectrum produced $R_1=2.03$ Å, $N_1=0.8$ and $R_2=3.26$ Å, $N_2=3.63$ for the two oxygen shells.

V. CONCLUSION

Well-ordered coadsorbed barium and oxygen overlayers that can form on the $W(100)$ surface include a stoichiometric layer with a $(\sqrt{2}\times\sqrt{2})R45^\circ=c(2\times 2)$ structure, and a layer with excess oxygen characterized by a $(2\sqrt{2}\times\sqrt{2})R45^\circ$ diffraction pattern. A stoichiometric barium and oxygen monolayer adsorbed

on tungsten may be viewed as a model of an active thermionic cathode surface.^{19,23} To minimize the work function a simple classical dipole picture of the surface favors a geometry in which barium and oxygen layers are displaced normal to the surface. Classically, a coplanar barium and oxygen geometry has no effect on the work function. Recent advances in the level of theoretical understanding for this adsorption system⁶⁻⁸ revealed that the work-function reduction is due to the polarization of the tungsten substrate by the barium atoms. The work function of the barium- and oxygen-covered surface is determined largely by the barium-to-surface separation. A perfectly coplanar barium and oxygen overlayer geometry can be consistent with the low value of the experimentally observed work function. On the $W(100)$ surface, a FLAPW total-energy calculation⁷ favors a tilted geometry with $\beta=74^\circ$ (16° off coplanar).

Recall that bond-length and coordination number information together with the long-range order of the $(\sqrt{2}\times\sqrt{2})R45^\circ$ overlayer imply a Ba-O internuclear displacement that is tilted with respect to the surface normal with $\beta=82^\circ$ —a value that is in good agreement with the FLAPW result. An oxygen shell with a barium-oxygen separation of 3.27 Å and $\beta=75^\circ$ was also present for the $(2\sqrt{2}\times\sqrt{2})R45^\circ$ overlayer. The coordination number for this oxygen shell was ~ 3.0 in the $(\sqrt{2}\times\sqrt{2})R45^\circ$ overlayer and ~ 3.6 for the $(2\sqrt{2}\times\sqrt{2})R45^\circ$ structure. These values are slightly less than the expected value of 4 for the tilted geometry. The difference may be due to the low accuracy of EXAFS coordination number determinations or the presence of vacancies in the ordered overlayers.

The binding energy of the oxygen 2s level is very sensitive to adsorption geometry. A recent ultraviolet photoemission spectroscopy (UPS) study of $(\sqrt{2}\times\sqrt{2})R45^\circ$ barium oxide overlayers on $W(100)$ (Ref. 11) measured an oxygen 2s binding energy that was consistent with the oxygen 2s binding energy predicted by FLAPW calculation for the tilted geometry. The measured binding energy was inconsistent with the oxygen 2s binding energy predicted for a “standing-up” geometry.²⁴

For the $(2\sqrt{2}\times\sqrt{2})R45^\circ$ overlayer the SEXAFS measurements indicate that there are ~ 0.8 excess oxygen atoms for each surface barium atom, in good agreement with the value of 0.9 determined from AES measurements. The adsorption site for the excess oxygen atoms lies outside the barium plane at a distance of 2.03 Å from the barium atoms. The Ba-O internuclear axis for these excess oxygen atoms is tilted $\sim 23^\circ$ from the surface normal. Although we do not know whether the excess oxygen atoms are above or below the barium layer on the basis of the SEXAFS measurements, due to spatial limitations beneath the barium layer we believe it is more likely that they adsorb above the barium plane.

The adsorption geometries proposed here for the $(\sqrt{2}\times\sqrt{2})R45^\circ$ and the $(2\sqrt{2}\times\sqrt{2})R45^\circ$ overlayers shown in Fig. 8 are similar to earlier adsorption models proposed on the basis of AES measurements.²⁵ The major difference is that for the nonstoichiometric overlayer the previous model placed the excess oxygen directly on top of the barium atoms. The present study indicates that

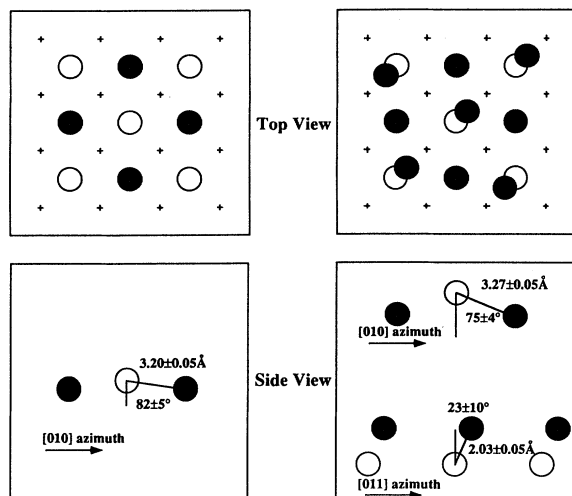
(a) $(\sqrt{2}\times\sqrt{2})R45^\circ$ Structure (b) $(2\sqrt{2}\times\sqrt{2})R45^\circ$ Structure

FIG. 8. The proposed adsorption geometries for the $(\sqrt{2}\times\sqrt{2})R45^\circ$ (left side) and the $(2\sqrt{2}\times\sqrt{2})R45^\circ$ (right side) overlayers. The open circles represent the barium atoms, the closed circles represent the oxygen atoms, while atoms of the tungsten surface layer are represented by crosses. Note that the adsorption sites of the barium and oxygen adatoms on the W(100) are unknown. A fourfold hollow site has been assumed for both here.

the O-Ba axis leans slightly (about 23°) with respect to the surface normal. This tilt provides a plausible mechanism to explain the occurrence of the $(2\sqrt{2}\times\sqrt{2})R45^\circ$ diffraction pattern: to minimize repulsion between the excess oxygen atoms, adjacent rows of Ba-O axes may tilt in opposite directions. The unit cell in one direction is thus twice the size of the unit cell of the $(\sqrt{2}\times\sqrt{2})R45^\circ$

structure and a $(2\sqrt{2}\times\sqrt{2})R45^\circ$ diffraction pattern is observed.

We have not determined the adsorption site of oxygen and barium for either of the overlayers due to the weakness of the tungsten backscattering. A technique other than SEXAFS may be more appropriate for this task. A possible approach may be to apply a backreflection x-ray standing-wave technique.²⁶

The adsorption geometries for a stoichiometric BaO layer previously proposed by Norman *et al.*⁴ and Shih *et al.*⁵ were different from the model presented here. Norman *et al.* proposed a standing-up model and Shih *et al.* proposed a tilted model with threefold symmetry. These two prior studies were performed on randomly oriented polycrystalline tungsten surfaces, in contrast with the W(100) single crystal in the present study. The difference in substrate leads to the drastically different SEXAFS results, and consequently the different adsorption models. The SEXAFS study described in this paper together with the results of LEED and UPS measurements and FLAPW calculations provided a detailed and consistent description of Ba and O adsorption geometries on W(100). A complete and reliable picture of the adsorption geometry on polycrystalline surfaces has to wait for the results of similarly careful studies with combined techniques on other single-crystal tungsten surfaces.

ACKNOWLEDGMENTS

A portion of this work was supported by the ONR 6.1 program. The authors wish to express their appreciation to Dr. Y. U. Idzerda for many illuminating discussions. The EXAFS measurements were performed on NSLS X23B, the NRL Materials Analysis beamline, designed and built by J. P. Kirkland, and R. A. Neiser. This research was carried out (in part) at the National Synchrotron Light Source, Brookhaven National Laboratory, which is sponsored by the U. S. Department of Energy, Division of Materials Sciences and Division of Chemical Sciences.

¹See, for example, J. Stohr, In *X-Ray Absorption, Principles, Applications, Techniques of EXAFS, SEXAFS and XANES*, edited by D. C. Koningsberger and R. Prins (Wiley, New York, 1988).

²E. A. Stern, B. Bunker, and S. M. Heald in *EXAFS Spectroscopy: Techniques and Applications*, edited by B. K. Teo and D. C. Joy (Plenum, New York, 1981).

³B. Bunker and E. A. Stern, *Phys. Rev. B* **27**, 1017 (1983).

⁴D. Norman, R. A. Tuck, H. B. Skinner, P. J. Wadsworth, T. M. Gardiner, I. W. Owen, C. H. Richardson, and G. Thornton, *Phys. Rev. Lett.* **58**, 519 (1987).

⁵A. Shih, C. Hor, D. Mueller, C. R. K. Marrian, W. T. Elam, P. Wolf, J. P. Kirkland, and R. A. Neiser, *J. Vac. Sci. Technol. A* **6**, 1058 (1988).

⁶L. A. Hemstreet, S. R. Chubb, and W. E. Pickett, *J. Vac. Sci. Technol. A* **6**, 1063 (1988).

⁷L. A. Hemstreet, S. R. Chubb, and W. E. Pickett *Phys. Rev. B* **40**, 3592 (1989).

⁸W. Muller, *IEEE Trans. Electron. Devices* **36**, 180 (1989).

⁹G. E. Moore and H. W. Allison, *J. Chem. Phys.* **23**, 1609 (1955).

¹⁰D. A. Gorodetsky and Yu. P. Melnick, *Bull. Acad. Sci. USSR, Phys. Ser.* **33**, 433 (1970).

¹¹D. Mueller, A. Shih, E. Roman, T. Madey, R. Kurtz, and R. Stockbauer, *J. Vac. Sci. Technol. A* **6**, 1067 (1988).

¹²R. A. Neiser, J. P. Kirkland, W. T. Elam, and S. Sampath, *Nucl. Instrum. Methods A* **266**, 220 (1988).

¹³D. E. Sayers and B. A. Bunker, in *X-Ray Absorption: Principles, Applications, Techniques of EXAFS, SAXAFS and XANES* (Ref. 1), Chap. 6.

¹⁴J. Stohr and R. Jaeger, *Phys. Rev. B* **27**, 5146 (1983).

¹⁵P. H. Citrin, *Phys. Rev. B* **31**, 700 (1985).

¹⁶J. Stohr, in *EXAFS and Surface EXAFS: Principles, Analysis and Applications*, edited by P. Day, NATO Advanced Study Institutes Ser. B: Physics (Reidel, Dordrecht, 1975), p. 59.

- ¹⁷E. A. Stern, D. E. Sayers, and F. W. Lytle *Phys. Rev. B* **11**, 4836 (1974).
- ¹⁸See, for example, R. W. G. Wyckoff, *Crystal Structures* (Interscience, New York, 1963 and 1965), Vols. I and III.
- ¹⁹G. A. Haas, a. Shih, and C. R. K. Marrian, *Appl. Surf. Sci.* **16**, 139 (1983).
- ²⁰A. G. McKale *et al.*, *J. Am. Chem. Soc.* **110**, 3763 (1988).
- ²¹P. H. Citrin,, P. Eisenberger, and R. C. Hewitt, *Phys. Rev. Lett.* **41**, 309 (1978); J. Stohr, R. Jaeger, G. Rossi, T. Kendelewicz, and I. Lindau, *Surf. Sci.* **134**, 813 (1983).
- ²²W. T. Elam, E. A. Stern, J. D. McCollum, and J. Sanders-Loehr, *J. Am. Chem. Soc.* **104**, 6369 (1982).
- ²³R. Forman, *Appl. Surf. Sci.* **2**, 258 (1979).
- ²⁴A. Shih, D. R. Mueller, and L. A. Hemstreet, *IEEE Trans. Electron. devices* **36**, 194 (1989).
- ²⁵See, for example, G. A. Haas, A. Shih, and C. R. K. Marrian, *Appl. Surf. Sci.* **16**, 157 (1983).
- ²⁶D. P. Wooduff, D. L. Seymour, C. F. McConville, C. E. Riley, M. D. Crapper, N. P. Prince, and R. G. Jones, *Phys. Rev. Lett.* **58**, 1460 (1987).